Computational investigation of ship propulsion performance in rough seas

P. Mizythras, E. Boulougouris & G. Theotokatos
University of Strathclyde, Glasgow, United Kingdom

ABSTRACT: In this paper, the performance of a merchant vessel propulsion system during acceleration is evaluated under different sea state conditions. The various parts of the main propulsion system have been modelled by using a mean value approach for the engine model with differential equations to calculate the engine crankshaft and turbocharger shaft speeds. Ship propulsion system has been modelled by using differential equations to calculate vessel speed and speed of advance. The output of the engine model has been validated under steady conditions according to the main engine shop test performance data. The calm water resistance is calculated following the ship sea trials results, whilst Wageningen polynomials have been used to simulate the propeller performance for the given hull resistance and speed. In order to estimate the added resistance for different weather conditions, the recommended procedures by International Standards have been followed. Then, the propulsion system performance is evaluated, both in calm water and waves, to investigate the main engine response during acceleration. Based on the simulation results, the propulsion system performance is discussed in respect for the engine response and vessel hydrodynamic performance, predicting the maximum vessel speed for the available engine power and speed.

KEYWORDS: marine Diesel engine; transient performance; propulsion system modelling; ship performance in various sea states; mean value engine modelling

1 INTRODUCTION

New policies and measures are introduced in order to improve energy efficiency and reduce fuel consumption in maritime industry (Bazari & Longva 2011). Instruments such as the energy efficiency design index (EEDI) and energy efficiency operational indicator (EEOI) have been introduced as indicators of the consumed energy. Their reference values (reference lines) are functions of size of the vessel, as indicated by its deadweight and its design speed at a nominal percentage of the installed main engine power. The formulation neglects the environmental impacts of the power requirements of the ship during transient acceleration or manoeuvring. Considering that many parameters can affect the selection of the installed engine power, new guidelines have been introduced to determine the minimum propulsion power in order to maintain the ships manoeuvrability (IMO 2015). Moreover, procedures have been established, aiming to improve ship performance assessment during sea trials, increasing the accuracy in the prediction of EEDI (ITTC 2014) and eliminating any measurement discrepancies.

However, the data gathered provide no indication of the engine's response at different sea states, loading conditions (trim and draught), or the maximum ship speed that is achievable with the selected engine power. All these conditions can vary significantly between different powertrain (e.g. engine, shafting, propeller) designs and affect the efficiency and the inherent safety margins. Based on these serious concerns, EU funded research project 'SHOPERA' was deployed, aiming at the development of suitable methods, tools and guidelines to address these issues (Papanikolaou et al. 2015).

For the simulation of the engine performance in transient conditions, several tools have been developed for specific case studies. A good example of such a tool, used for real-time simulation of a COGAG ship propulsion system has been presented by (Altosole et al. 2008). It is also able to predict the propulsion system dynamics during manoeuvring (Viviani et al. 2008). Taskar et al. studied the performance of the coupled propeller-engine system in waves (Taskar et al. 2016). Their results provide a good insight on the engine-propeller dynamics performance, with special focus to the propeller

inflow velocity for different wave profiles. Other efforts include the estimation of the engine's performance and the fuel consumption based on the assumption of ship resistance increase due to various factors (e.g. sea state, hull fouling) (Theotokatos & Tzelepis 2015), whilst several studies have attempted to simulate the propulsion system performance, using simplifying assumptions for the resistance through the use of a standard resistance curve (Kyrtatos et al, 1999; Theotokatos 2010) or based on ship motions and model test results (Zhao et al. 2015).

Considering the necessity for further studying in these dynamic phenomena and the limited research on this field, this paper focuses on the development of a new model that will investigate the performance of propulsion system, consisting of a two-stroke, turbocharged, marine Diesel engine, during acceleration in various sea states. In order to balance the method's accuracy and the complexity of the required input data for each simulation, semi-empirical methods were used and validated with ship trial tests investigating the engine response to the hydrodynamic performance of ship.

2 SHIP PROPULSION SYSTEM MODELLING

The studied propulsion system consists of a marine diesel engine coupled to the ship's propeller through the shafting system. For the ship of the present study, a two-stroke, turbocharged, marine Diesel engine, has been simulated, delivering power through direct drive connection to a fixed pitch propeller.

Various methods are available for the estimation of ship resistance in calm water. Experimental data provide the most accurate solution for the prediction of the resistance for the specific ship but in lack of these, semi-empirical formulae can be used to estimate the ship resistance, according to the main particulars of the ship. In this case study, the regression analysis of the trial data has been chosen for the prediction of ship resistance in calm water.

Considering that marine vessel does not always sail in calm water, different sea states have to be simulated. The majority of ocean waves are triggered by wind (ITTC 2002) Therefore, wind speed can be used as the main variable for the definition of sea state with the assumption that the wind speed is constant during ship sailing and ship sails in fully developed seas. Based on the sea state parameter, the added resistance in waves is calculated by using semi-empirical methods, providing fast solutions and reasonably accurate results.

The authors have developed a code encapsulating all the above, modelling both the ship propulsion and resistance of a ship. This has been developed in MATLAB®. The main objective of this model is to predict adequately the ship performance and acceleration in various conditions, using only limited input data.

2.1 Engine model description

The current model for the engine is based on the previous work presented by (Theotokatos 2010). This mean value engine model is a simple and computationally light model, providing sufficiently accurate estimation of the engine performance. Due to its simplicity, mean value model was used along with an external compressor map method to cover engine performance in partial load conditions (Guan et al. 2014) or combined with zero-dimensioned model in order to predict in-cylinder parameters (Baldi et al. 2015).

The input variables for the engine model are the engine speed and the rack position, corresponding to the shaft's rotation and the engine's governor position respectively. The main engine components, such as cylinders and turbocharger, scavenging and exhaust receivers, air cooler and auxiliary air blower, as well as the exhaust pipe and air filter have been modelled by following thermodynamic and fluid dynamics principles. A detailed description of engine model is given by Theotokatos (2010).

2.2 Compressor performance map extension model description

Compressor performance maps provided by manufacturers cover the rotational area from 40% to 100% of the maximum turbocharger speed. Due to the partial load operation of the engine, the turbocharger will operate at low speeds. As a result, the compressor's performance map needs to be extended to lower turbocharger speeds. An attempt to use an extended compressor map in the mean value engine model has been achieved by Guan et.al. (Guan et al. 2014). In the present model, a similar approach was used, introducing some alterations for the calculation of compressor pressure ratio as a function of the volumetric flow rate. The input data for this model is the turbocharger's shaft speed and the compressor's pressure ratio, whereas the output data include the air volumetric flow rate and the isentropic efficiency coefficient.

The compressor performance map can be described with the non-dimensional parameters φ, Ψ and M_{in}. The compressor's non-dimensional flow and isentropic head coefficients (φ and Ψ respectively) are defined as (Yahya 2010):

$$\varphi = \frac{\dot{V}_C}{A_C U_C} \tag{1}$$

$$\Psi = \frac{pr_C^{\frac{\gamma_a - 1}{\gamma_a}} - 1}{(\gamma - 1) M_{in}^2} \tag{2}$$

where U_C is the compressor impeller tip velocity and M_{in} is the compressor impeller tip Mach velocity, given from the respective formulae (Yahya 2010):

$$U_C = \pi N_{TC} D_{C\_tip} \quad (3)$$

$$M_{in} = \frac{U_C}{\sqrt{\gamma R_a T_{amb}}} \quad (4)$$

Justified by numerical and experimental results, Greitzer and Moore (Greitzer & Moore 1985) suggested a single cubic polynomial to describe the compressor map. This approach has been successfully applied in a vast number of studies that used similar polynomial approximations (Meuleman et al. 1998). The polynomial is described by the following equation:

$$\Psi(\varphi) = \Psi(0, M_{in}) + k_H(M_{in})\left[1 + \frac{3}{2}\left(\frac{\varphi}{k_W(M_{in})} - 1\right) - \frac{1}{2}\left(\frac{\varphi}{k_W(M_{in})} - 1\right)^3\right] \quad (5)$$

The parameters $\Psi(0,M_{in})$, $k_H(M_{in})$ and $k_W(M_{in})$, can be determined from steady-state compressor map and subsequently interpolated by polynomials as function of M_{in} (Willems 2000). The procedure for the polynomial approximation is described by van Helvoirt (van Helvoirt 2007). Following the aforementioned method, the compressor pressure ratio is expressed as a function of volumetric flow rate and turbocharger speed.

The compressor isentropic efficiency at low turbocharger speed is calculated according to the method, given by Guan (Guan et al. 2014).

2.3 Propeller model description

The ship propeller torque and thrust are calculated by using the non-dimensional torque and thrust coefficients respectively, the sea water density, the propeller rotational speed and the propeller diameter:

$$Q_P = K_Q \rho_{sw} N_P^2 D_P^5 \quad (6)$$

$$T_P = K_T \rho_{sw} N_P^2 D_P^4 \quad (7)$$

The non-dimensional torque and thrust coefficients in open-water conditions are calculated using the polynomials of Wageningen B-screw series (Oosterveld & Van Oossanen 1975), as a function of propeller characteristics (pitch-to-diameter ratio at 70% of propeller radius, expanded area ratio and number of blades) and advance coefficient. The propeller advance speed coefficient is given by the formula:

$$J_P = \frac{60 U_A}{N_P D_P} \quad (8)$$

where speed of advance U_A is calculated with the method described in Section 2.4.

In order to increase the model's accuracy, the non-dimensional torque and thrust coefficients have been corrected according to the ship propulsion data with correction factors, described as polynomial functions of advance speed coefficient:

$$k_{K_Q} = k_{Q0} + k_{Q1} J_P^3 \quad (9)$$

$$k_{K_T} = k_{T0} + k_{T1} J_P^2 + k_{T1} J_P^4 \quad (10)$$

The propeller open water efficiency is defined by the formula:

$$\eta_P = \frac{K_T J_P}{2\pi K_Q} \quad (11)$$

When the propeller rotates underwater, the propeller inertia is increased due to the water mass entrained into the propeller. The added inertia due to the entrained water can be found only after experiments but semi-empirical formulae are available which estimate this increase to the actual propeller inertia (Korotkin 2009). In terms of this study, the propeller inertia out of water and added inertia of entrained water are collected by the ship trial data:

$$I_{P\_tot} = I_{P\_act} + I_{P\_entr} \quad (12)$$

2.4 Propulsion model description

Propulsion system is simulated by modelling the propeller dynamics. Yoerger (Yoerger et al. 1990) provided a model which describes the dynamics of sub-merged vehicle thrusters. This one-state model is based on the assumptions that the propeller acts as an actuator disk in a thrust tunnel, fluid is incompressible and friction losses, rotational flow and gravity effects are ignored. The governing equations are:

$$T_P = \frac{\dot{V}_P(t)|\dot{V}_P(t)|}{\rho_{SW} A_P} \quad (13)$$

$$\omega_P Q_P = \frac{\rho_{SW} V_s}{A_P^2} \ddot{V}_P(t) q(t) + \frac{\rho_{SW}}{2A_P} \dot{V}_P^2(t) \left|\dot{V}_P(t)\right| \quad (14)$$

where $\dot{V}_P(t)$ is the volumetric flow rate of sea water that pass through the propeller:

$$\dot{V}_P(t) = A_P U_A \quad (15)$$

Taking into account the influence of the fluid mass in the tunnel and its associated hydrodynamic mass, McLean (McLean 1991) improved this model to the following one:

$$T_P = \rho_{SW} L_P (1 + K_a) \ddot{V}_P(t) + \frac{\rho_{SW} \Delta k_\beta}{A_P} \dot{V}_P(t) \left|\dot{V}_P(t)\right| \quad (16)$$

$$\omega_P Q_P = \frac{\rho_{SW} L_P (1 + K_a) k_\beta}{A_P} \dot{V}_P(t) \ddot{V}_P(t) + \frac{\rho_{SW} \Delta k_\alpha}{2A_P^2} \dot{V}_P^3(t) \quad (17)$$

where k_β and k_α are the nondimensional momentum and energy flux correction factor of the flow respectively (White 2009). As a result, the difference of these correction factors can estimate the fluid flow disturbance due to the presence of the propeller. During the simulation, the difference of nondimensional momentum flux factor is given as a polynomial function of engine's rotational speed and

the results have been validated with the wake fraction coefficient derived from the ship's sea trial data in calm water. It shall be noted that during the simulations in rough seas, the effect of sea state or ship heave motions to the fluid flow profile are neglected, assuming that the dimensionless momentum flux depends only on the engine's speed.

Substituting Equation 15 into Equation 16, a differential formula for the calculation of speed of advance derives:

$$\frac{dU_A}{dt} = \frac{T_P}{m_{SW}} - \frac{\rho_{SW} A_P \Delta k_\beta}{m_{SW}} U_A |U_A| \quad (18)$$

In this differential equation, the mass of entrained sea water m_{SW} is used. This is equal to the fluid volume of a cylinder with diameter and length equal to the propeller diameter, plus the added water mass in propeller as it is estimated by Schwanecke theory (Carlton 2012):

$$m_{SW\_entr} = 0.2812 \frac{\pi \rho_{SW} D_P^3}{z} \left(\frac{A_e}{A_P}\right)^2 \quad (19)$$

The forward speed of the vessel V_s, is calculated by solving the ship surge motion differential equation:

$$\left(m_s + m_{hydro}\right) \frac{dU_S}{dt} = (1-t)T_P - RR_{S\_tot} \quad (20)$$

In this differential equation, the total resistance consists of three components:

$$RR_{S\_tot} = RR_{S\_CW} + RR_{S\_AWV} + RR_{S\_AWI} \quad (21)$$

The first term corresponds to the calm water resistance. Due to the ship performance data availability, calm water resistance is expressed as a polynomial function of vessel speed instead of using any other semi-empirical method, improving the overall simulation accuracy:

$$RR_{S\_CW} = k_{RR1} U_S^{k_{RR2}} \quad (22)$$

where constants k_{RR1} and k_{RR2} are estimated based on the ship trial data.

Added resistance due to wave RR_{S_AWV} and wind RR_{S_AWI} are calculated with the assumption that vessel sails in head seas. For the estimation of added wave resistance, the STAWAVE-2 model has been applied (van den Boom et al. 2013). STAWAVE-2 is a semi-empirical model developed by MARIN and it is one of the methods selected from ITTC and IMO for the estimation of the added water resistance and the correction of the total resistance during the assessment of vessel power performance (IMO 2013; ITTC 2014).

This method is very simple and it is the result of experimental data collected from various ships under different wave profiles. The required input for the estimation of added resistance includes the main particulars of the ship (e.g. length, draught) and the wave profile characteristics (e.g. amplitude, length, frequency). The estimation of wave profile characteristics is described in Section 2.5.

Considering that only the surge motion of ship is simulated in head waves, this semi-empirical method provides sufficient estimation of the additional resistance with the assumption that the other ship motions have no coupling effects. Potential theory by using far-field or near-field methods (Papanikolaou & Liu 2010) could provide more accurate results for a specific vessel, but at the expense of computational cost and model complexity.

Finally, the added wind resistance is measured by using a physical-component-method, developed by Fujiwara (Fujiwara et al. 2006). Wind resistance coefficient is given as a function of the relative wind angle, vessel main particulars and the exposed areas above the waterline in the lateral and transverse direction. A correction has been applied for the final value of the wind resistance load, taking into account the relative motion between the vessel and the wind. Resistance increase due to other parameters such as hull roughness or trim conditions is currently neglected.

Ship mass includes both the displacement mass, and the added hydrodynamic mass in surge. The latter is used in order to include the developed hydrodynamic force due to the surge acceleration of a body in the fluid. This hydrodynamic added mass is estimated empirically by following the Sargent and Kaplan method (Journée 2001; Sargent & Kaplan 1974) as a percentage of the ship's total mass.

When the vessel's speed and the propeller's speed of advance are calculated, the dynamic wake fraction of the ship can be estimated by the following formula:

$$w = \frac{U_S - U_A}{U_S} \quad (23)$$

The thrust deduction coefficient, defined by Equation 24, is estimated by Equation 25 as a function of ship's wake fraction and thrust loading coefficient (Tsakonas 1958):

$$t = \frac{T_P - R_{S\_tot}}{R_{S\_tot}} \quad (24)$$

$$t = 2\left[\frac{-1+(1+k_T)^{1/2}}{C_T}\right]\frac{w}{1-w} \quad (25)$$

Thrust loading coefficient is given by the formula:

$$k_T = \frac{T_P}{\frac{1}{2}\rho_{SW} U_A^2 A_P} \quad (26)$$

Based on the wake fraction and the thrust deduction coefficient, the ratio of effective power to thrust power, defined as hull efficiency, is calculated as follows:

$$\eta_H = \frac{1-t}{1-w} \quad (27)$$

Shaft efficiency, η_{Sh}, is taken as constant in the system, estimated by ship propulsion data, whereas the overall propulsive efficiency is given by the following equation (Carlton 2012):

$$\eta_D = \frac{\pi N_P Q_P}{30 P_B} = \eta_H \eta_R \eta_P \eta_{Sh} \quad (28)$$

Based on the overall propulsive efficiency, the propeller relative rotative efficiency η_R can be estimated.

2.5 Sea state model description

In order to estimate the sea loads and responses for each sea state, a wave model has to be applied. Sea states are most often specified by the short-term variance spectrum of the elevation of a point. For the sea state description, various spectral formulations have been presented (ITTC 2002).

Main spectra parameters are the significant wave height and a characteristic wave period, defined by the spectrum. Alternative spectra, such as the JONSWAP model (Hasselmann et al. 1973), take into consideration additional parameters, such as the fetch length and shaper parameters, for a better approximation of field measurements. In terms of this study, a simple wave spectrum is used for the sea state modelling, namely the Pierson and Moskowitz spectrum (Pierson & Moskowitz 1963), which corresponds to fully developed seas. Based on these wave characteristics and assuming that ship sails in deep water, the wave length is calculated, describing the wave profile that is applied on the ship.

Bearing in mind that wind load depends only on wind speed and direction, and assuming that the ship sails under constant wind speed, wind direction and on full developed head seas, the overall sea state can be described as a function of wind speed. In order to avoid thrust losses when propeller operates close to the free surface as the ship oscillates in waves, the minimum immersion of propeller shaft at the worst case scenario was kept at 130% of the propeller radius (Minsaas et al. 1983).

3 MODEL CASE STUDY

3.1 Propulsion system model set up

In this study, an Aframax crude oil tanker vessel was investigated. The vessel has deadweight of 115000 MT, powered by MAN 7S60MC-C, a two-stroke, turbocharged, marine Diesel engine. One turbocharged unit is used, whereas an air cooler unit is installed between the compressor and the inlet receiver to increase the engine's efficiency. The main engine is directly connected to a fixed pitch 4-blade propeller. The main particulars of the ship, its engine and propeller are summarized in Table 1, collected from the ship sea trials and engine shop tests.

In order to set up the model for the selected ship, the geometric data of the propeller and engine, the performance curves of the air blower, air cooler and turbocharger, as well as experimental data of the main engine performance have been used. Polynomial regression models were used to set up the engine model, deriving from the engine shop tests.

Table 1. Ship propulsion system parameters.

Ship parameters		
Type	Crude oil tanker	
Size	115000	MT
Length overall	250	m
Breadth	43.8	m
Depth	21.3	m
Draught	14.9	m
Displacement	134005	m^3
Propulsion engine parameters		
Engine type	MAN 7S60MC-C	
Number of cylinders	7	
Bore	600	mm
Stroke	2292	mm
Brake power (MCR*)	14250	kW
Engine speed (MCR*)	110	r/min
BMEP** (MCR*)	17.9	bar
Turbocharger unit	1 x MHI	
Propeller parameters		
Type	Fixed pitch	
Diameter	7.4	m
Number of blades	4	-
Pitch	4.8	m
Expanded area	22.2	m^2

*MCR: maximum continuous rating
**BMEP: brake mean effective pressure

Engine speed is given as the PI controller input variable for the fuel governor. During the simulation of the engine's performance under various sea states, a speed slope limiter was selected based on the available data. The speed slope limiter aims to the engine's protection during the acceleration and deceleration of ship under actual conditions. These values are given in Table 2.

The fuel that was used for the simulation was assumed to be low Sulphur heavy fuel oil (LSHFO) type, with a lower heating value equal to 42.7 MJ/kg. For the detailed modelling of ship propulsion and the accurate estimation of vessel resistance, the main particulars and hydrodynamic data from ship trials were used. Based on the available information, the wake velocity profile of the flow at the propeller was set-up through a trial and error procedure. All the models that describe the ship propulsion model are validated in calm water for steady state conditions.

Table 2. Engine speed acceleration/deceleration slope limits.

	Acceleration slope (r/min/s)	Deceleration slope (r/min/s)
Engine speed < 58 r/min	0.04	0.08
Engine speed ≥ 58 r/min	0.015	0.03

3.2 Validation process

During the validation process for the engine model, engine performance was simulated for the range from 25% to 100% of the maximum continuous rating (MCR) point, based on the available data. In this case, only the engine system model was used, by setting as input variables the rack position and the engine crankshaft speed that were indicated from the measurements, neglecting the effects from the propeller or the ship to the engine.

The best accuracy of engine model is achieved at the load range from 75% to 100% of engine MCR, where the minimum error is present (error < 4%). In lower loads, even though the error increases, the accuracy of the model is still satisfactory (error < 8%)

The overall propulsion model was validated using the ship hydrodynamic performance at various speeds, as it was recorded during the trials for various crankshaft engine speeds. The trials were performed in calm sea water conditions. In order to simulate the sea conditions during trials, the wind speed was set to zero (0 m/s) whilst the engine speed at each tested case was given as the required speed for the propulsion system model. The simulation was performed till every engine parameter reached the steady state conditions and then the final hydrodynamic results were compared to the sea trial measurements. Based on the results, it was proven that the model used for the prediction of the speed of advance gives accurate results in calm sea water conditions.

The validation process proved that the overall propulsion model represents the actual ship response predicting total resistance, vessel speed, and wake fraction and thrust deduction factors with adequate accuracy.

4 RESULTS

Based on the satisfactory results of validation process, the developed model is used to investigate the overall ship performance under different sea states. As it was described in Section 2.5, the sea states are given as a function of wind speed and wind incident angle. During the simulation, the head wave and wind angles remain constant and equal to zero degrees throughout the calculations.

Considering that the main objective of this study is to estimate the acceleration of the ship under different sea state conditions, the simulation was performed for the acceleration from a constant vessel speed to the maximum achievable speed for the given sea conditions. For the initial condition, it was assumed that the ship was sailing with a speed of 5 knots that provides adequate manoeuvrability under any sea state. The simulation ends when the engine reaches the MCR point and the vessel's speed value converges.

The initial engine speed was selected by following an iterative process, in order to obtain the speed that satisfied the initial conditions in terms of vessel speed. Then, the model was run for 30 seconds in steady conditions, under the initial speed that was set manually. After that, the maximum engine ordered speed of 110 r/min was set to the governor, following the acceleration slope which has been introduced to the model. During the simulation, the acceleration to the MCR point is assumed to be performed without pauses, simulating an emergency condition.

In Figure 1, the total resistance, the vessel's speed, the break specific fuel consumption, the exhaust gas receiver temperature, the air-fuel equivalence ratio and the turbocharger speed are presented versus time. As it was expected, when the sea state increases, the total resistance increases for the same initial vessel speed. Comparing the vessel speed with the total resistance diagrams, it is obvious that vessel speed and total resistance diagrams have the same curvature against time, till the moment that vessel has achieved its maximum available speed.

The vessel speed is depicted in Figure 1b. According to this diagram, when the wind speed and the wave amplitude increases the maximum vessel speed decreases. Also, the acceleration slope is different for each sea state. The reason is the initial engine speed that was set for each sea state condition and the speed slope limiter that has been applied to the engine. When the ship sails in calm water, the engine is capable to deliver the desired vessel speed at lower crankshaft speed. Due to the standard slope limiter, the acceleration at low engine speed is slower than at higher speeds. On the other hand, when the engine operates at greater speeds, then the acceleration slope is greater, allowing to the engine to increase the vessel's speed faster. Even though the acceleration is greater in harsh sea conditions, the maximum engine rotational speed is not adequate to provide enough power to the vessel to achieve the design speed.

In Figure 1c the brake mean effective pressure (BMEP) versus time is presented. In extremely low speed operation, the engine operates in high BSFC. When the engine load increases to 25% approximately, BSFC decreases, whereas from the low to medium engine load, the specific fuel consumption increases. When the engine load is over 50%, and before engine reaches its maximum

speed limit, BSFC increases due to the increased fuel mass flow rate that is injected into the cylinders.

The air-fuel equivalence ratio is high when engine operates in low speed and loads (Fig. 1e). When the engine load increases, the air-fuel equivalence ratio decreases, representing the fuel mass flow rate increase. Due to the increased fuel mass flow rate, the exhaust gas receiver temperature increases (Fig. 1d) and as a result, the turbocharger speed increases (Fig. 1f), providing additional air to the engine cylinders.

It must be noted that when the speed slope limiter increases in higher engine speeds, then a 'jump' is present at the exhaust gas temperature diagram due to the greater rate of injected fuel into the cylinders. This increase of the exhaust gas temperature at the exhaust gas receiver increases the acceleration rate of the turbocharger speed. When the overall system is stabilized after the change of the engine speed slope limiter, the examined engine performance parameters increase till the engine reaches its MCR point.

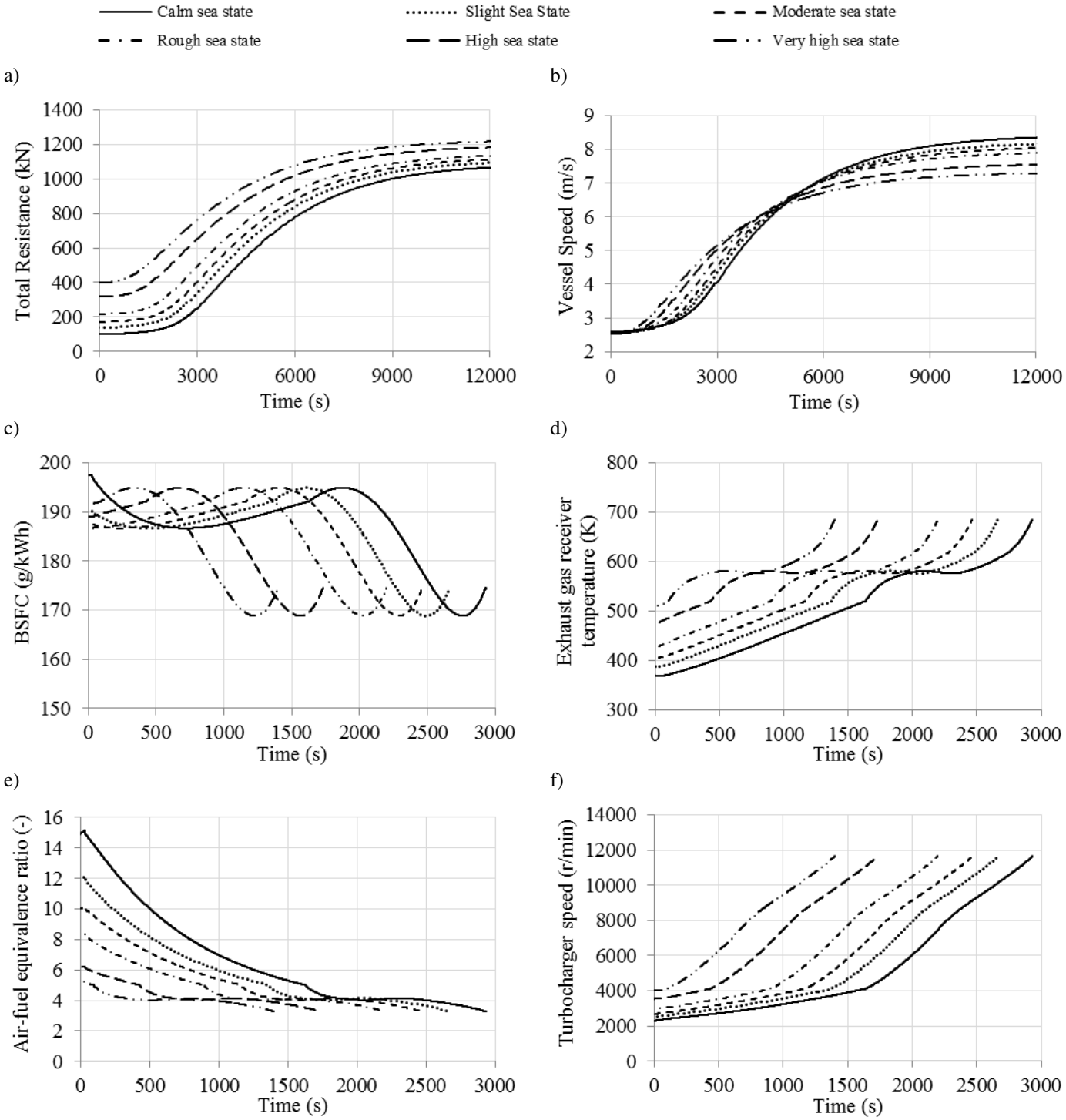

Figure 1. Ship performance time diagrams for a) Total resistance, b) Vessel speed, c) Brake specific fuel consumption (BSFC), d) Exhaust gas receiver temperature, e) Air fuel equivalence ratio and f) Turbocharger speed in various sea states.

Comparing the results at different sea states, the engine parameters diagrams and the speed of advance have the same slope when the sea state changes, with only difference to be present on the initial point. This difference is caused due to the assumption that the vessel starts its acceleration from a fixed speed, but for a different speed for the engine crankshaft. Also, when the speed slope

limiter changes, a reasonable time is required for the engine to identify the new operational conditions and engine components performance to be restored due to the turbocharging system lag.

For the different sea states, the maximum speed that can be achieved by the vessel is presented in Table 3. Also, in the same table, the sea state profiles of the simulation are described, identifying the significant wave height, frequency and length, for the defined wind speed based on the Pierson-Moskowitz wave spectrum.

Table 3. Sea state parameters and maximum vessel speed

Sea state	Wind speed (m/s)	Wave frequency (s^{-1})	Wave height (m)	Wave length (m)	Maximum vessel speed (knots)
Calm	0	-	0	-	16.41
Slight	7.45	0.232	1.25	28.99	16.02
Moderate	10.55	0.164	2.50	58.13	15.76
Rough	13.35	0.130	4.00	93.09	15.46
High	18.90	0.092	8.02	186.57	14.77
Very high	23.10	0.075	11.98	278.70	14.27

As it was presented in Figure 1, the vessel requires for each case more than quadruple time to reach the maximum available speed in comparison with the required time for the engine to achieve MCR point. In order to reduce the computational time for the calculation of vessel speed and hydrodynamic parameters, and taking into account that the engine has achieved the maximum speed, a 'virtual acceleration' coefficient has been applied, speeding up the computational process.

The delayed acceleration of ship under calm water sea state conditions in comparison with the engine is presented at the thrust deduction and wake fraction factors, shown in Figures 2 and 3, respectively. Both figures prove that the propeller, following the engine acceleration, generates the maximum thrust and speed of advance faster. As a result, the thrust deduction and wake fraction decrease till the moment that the engine reaches the MCR point. After this point, the factors increase back to their steady state value. Also, the change at the speed slope limiter of the governor is presented at the negative slope of both factors, confirming the importance of the fuel rack position to the performance of the ship.

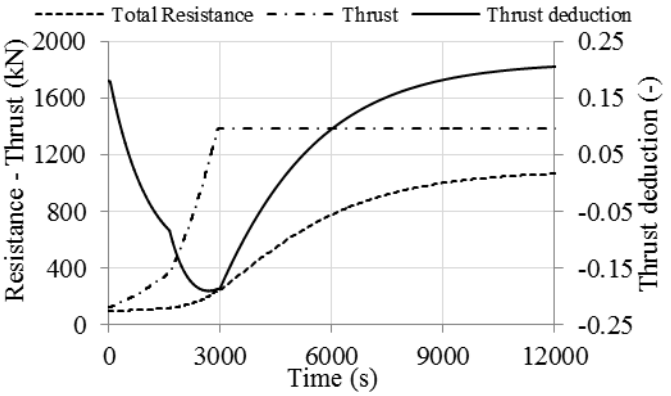

Figure 2. Thrust deduction factor and comparison between resistance and thrust versus time in calm water.

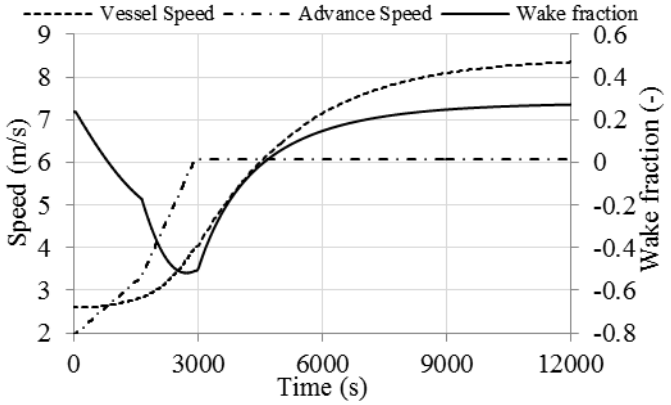

Figure 3. Wake fraction factor and comparison between vessel speed and speed of advance versus time in calm water.

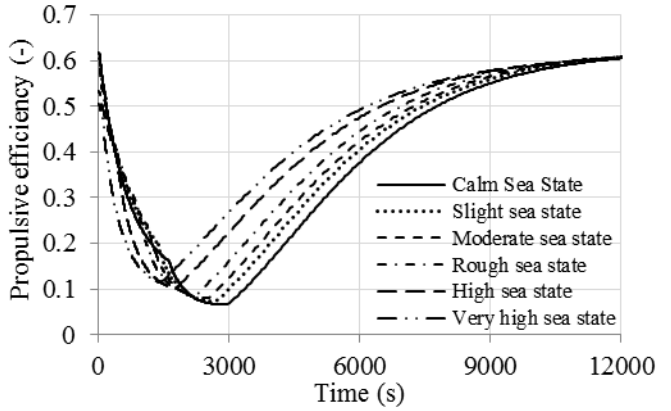

Figure 4. Overall propulsive efficiency versus time for carious sea states.

Finally, in the Figure 4, the overall propulsive efficiency is presented for each investigated sea state. Due to the low values of wake fraction and thrust deduction factors during engine acceleration and considering that open water propeller efficiency and shaft efficiency remain constant, the propulsive efficiency decreases. The minimum propulsive value is calculated when propeller provides the maximum speed and thrust to the ship but the vessel speed and total resistance are still low. When the ship accelerates, and both the vessel's speed and the resistance increase, then the overall efficiency increases.

5 CONCLUSIONS

In this study, a propulsion model using limited data as input was presented, capable of investigating the coupled engine-propeller-ship system during transient conditions such as the acceleration of the ship. The model was based on thermodynamic principles and simplified hydrodynamic theories, programmed in Matlab®. The transient engine performance was investigated in various sea states, identifying the engine response during acceleration, the maximum obtainable vessel speed for different sea states under head waves and the interconnections between ship propeller hydrodynamic performance and engine response.

The developed mean value engine model is proved to represent adequate efficiently the engine performance under various loads. Also, the propeller dynamics method implemented in the model predict adequately the dynamic performance of propeller. Finally, the Pierson-Moskowitz wave spectrum that was used for the generation of wave profile and identification of wave characteristics, estimates the sea state only by using the wind speed as input parameter.

Based on the simulation results, the maximum vessel speed decreases when the ship sails in rough seas and the resistance increases as it was expected. Taking into account that governor speed slope during acceleration is constant for all the investigated cases, and that the engine needs to operate in higher speed to deliver the required vessel speed in rough seas, the ship accelerates faster.

For the simulation runs, an engine speed slope limiter has been applied in addition to the governor limiters in respect of engine speed and scavenging air pressure. Based on the results, it is noted that PI controller and fuel rack position are crucial during ship propulsion and acceleration, affecting not only the behaviour of propulsion system components, but the hydrodynamic performance of propeller as well.

Besides the selection of the speed slope limiter, the propeller wake is an additional crucial factor for the successful simulation of the engine's response. In this study, the wake profile was validated only in calm water sea state conditions. A more advanced model of the propeller performance in the waves, or an analytical simulation of the flow at the propeller, is possible to provide more accurate results for the total response of the engine during acceleration under different conditions.

Finally, the importance of engine control through the governor was presented. The decision of the fuel amount that will be injected into the cylinders every moment and the operational point where engine is optimized has great effect under rough seas or emergency conditions. As a result, the maximum or the minimum required power of the engine is not the only critical issue that needs to be investigated for each vessel, but also the response of the engine on transient conditions.

Considering the engine response, additional operational or design solutions can be provided to improve engine performance, such as the use of a speed slope limiter with steeper slope at the engine governor, the application of turbocharger cut-out at low loads, the installation of an additional smaller turbocharger during part load operation, or the use of a diesel-electric propulsion system.

ACKNOWLEDGEMENT

This work was performed within the H2020 project "HOLISHIP-Holistic Optimisation of Ship Design and Operation for Life Cycle" which was funded by the EU under contract 689074.

NOMENCLATURE

Notations	
A	area (m^2)
D	diameter (m)
I	polar moment of inertia (kg m^2)
J	propeller advance speed (m/s)
k	coefficient
K_a	proportion of entrained sea water mass in propeller
K_Q	non-dimensional torque coefficient
K_T	non-dimensional thrust coefficient
L	length (m)
m	mass (kg)
$\dot{m}$	mass flow rate (kg/s)
M	Mach number
N	rotational speed (r/min)
pr	pressure ration
Q	torque (Nm)
R	gas constant (J/kg K)
RR	resistance (N)
T	temperature (K)
t	thrust deduction factor
T_P	propeller thrust (N)
U	speed (m/s)
V	volume (m^3)
$\dot{V}$	volumetric flow rate (m^3/s)
$\ddot{V}$	time first derivative of volumetric flow rate (m^3/s^2)
w	wake fraction factor
Greek symbols	
α	flow coefficient
γ	ratio of specific heats
Δ	difference of units

η	efficiency
ρ	density (kg/m^3)
φ	non-dimensional flow coefficient
Ψ	non-dimensional isentropic head coefficient

Abbreviations	
a	air
amb	ambient
A	advance
AWI	added wind
AWV	added wave
C	compressor
CW	calm water
eff	effective
$entr$	entrained
h	hull
$hydro$	hydrodynamic added
P	propeller
R	rotative
S	ship
SC	scavenging receiver
SW	Sea water
TC	turbocharger
tot	total

REFERENCES

Altosole, M. et al., 2008. Real-time simulation of a COGAG naval ship propulsion system. Proceedings of the Institution of Mechanical Engineers, Part M: Journal of Engineering for the Maritime Environment, 223, pp.47–62.

Baldi, F., Theotokatos, G. & Andersson, K., 2015. Development of a combined mean value–zero dimensional model and application for a large marine four-stroke Diesel engine simulation. Applied Energy, 154, pp.402–415.

Bazari, Z. & Longva, T., 2011. Assessment of IMO Mandated Energy Efficiency Measures for International Shipping: Estimated CO2 Emissions Reduction from Introduction of Mandatory Technical and Operational Energy Efficiency Measures for Ships.

van den Boom, H., Huisman, H. & Mennen, F., 2013. New Guidelines for Speed/Power Trials. Level playing field established for IMO EEDI. SWZ Maritime, pp.1–11.

Carlton, J.S., 2012. Marine Propellers and Propulsion, 3rd ed., Butterworth-Heinemann.

Fujiwara, T., Ueno, M. & Ikeda, Y., 2006. Cruising Performance of a Large Passenger Ship in Heavy Sea. Engineering Conference, 4, pp.304–311.

Greitzer, E.M. & Moore, F.K., 1985. A Theory of Post-Stall Transients in Axial Compression Systems, NASA Contractor Report, 108(March 1985), p.120.

Guan, C. et al., 2014. Computational investigation of a large containership propulsion engine operation at slow steaming conditions. Applied Energy, 130, pp.370–383.

Hasselmann, K. et al., 1973. Measurements of Wind-Wave Growth and Swell Decay during the Joint North Sea Wave Project (JONSWAP), Hamburg.

van Helvoirt, J., 2007. Centrifugal Compressor Surge: Modelling and Identification for Control. PhD Thesis, Technische Universiteit Eindhoven.

IMO, 2015. The Marine Environment Protection Committee, Circular MEPC.1/Circ.850/Rev. 1, 2013 Interim Guidelines for determining minimum propulsion power to maintain the manoeuvrability of ships in adverse conditions, as amended.

IMO, 2013. The Marine Environment Protection Committee, RESOLUTION MEPC.234(65), Amendments to the 2012 Guidelines on Survey and Certification of the Energy Efficiency Design Index (EEDI) (Resolution MEPC.214(63)), as amended.

ITTC, 2002. The Specialist Committee on Waves Final - Report and Recommendations to the 23rd ITTC, Proceedings of 23rd ITTC.

ITTC, 2014. Recommended Procedures and Guidelines - Speed and Power Trials, Part 2 - Analysis of Speed/Power Trial Data.

Journée, J., 2001. Theoretical Manual of SEAWAY, The Netherlands.

Korotkin, A.I., 2009. Added masses of ship structures, Springer.

Kyrtatos, N.P. et al., 1999. Simulation of the overall ship propulsion plant for performance prediction and control. MarPower99 Conference.

McLean, M.B., 1991. Dynamic Performance of Small Diameter Tunnel Thrusters. MSc Thesis, Naval Postgraduate School.

Meuleman, C. et al., 1998. Surge in a low-speed radial compressor. International Gas Turbine and Aeroengine Congress.

Minsaas, K., Faltinsen, O.M. & Persson, B., 1983. On the importance of added resistance, propeller immersion and propeller ventilation for large ships in a seaway. 2nd international symposium on practical design in shipbuilding. Tokyo & Seoul.

Oosterveld, M.W.C. & Van Oossanen, P., 1975. Further computer-analyzed data of the Wageningen B-screw series. International Shipbuilding Progress, 22(479), p.13.

Papanikolaou, A. et al., 2015. Energy Efficient Safe Ship operation (SHOPERA). 12th International Marine Design Conference - IMDC, (May).

Papanikolaou, A. & Liu, S., 2010. On the Prediction of Added Resistance of Ships in Waves. William Froude Conference: Advances in Theoretical and Applied Hydrodynamics – Past and Future. Portsmouth, UK.

Pierson, W.J. & Moskowitz, L., 1963. A proposed spectral form for fully developed wind seas based on the similarity theory of S. A. Kitaigorodskii. U.S. Naval oceanographic Office, (N62306-1042).

Sargent, T.P. & Kaplan, P., 1974. Modifications to Lloyds Register of Shipping Strip Theory Computer Program (LR 2570).

Taskar, B. et al., 2016. The effect of waves on engine-propeller dynamics and propulsion performance of ships. Ocean Engineering, 122, pp.262–277.

Theotokatos, G., 2010. On the cycle mean value modelling of a large two-stroke marine diesel engine. Proceedings of the Institution of Mechanical Engineers, Part M: Journal of Engineering for the Maritime Environment, 224(3), pp.193–205.

Theotokatos, G. & Tzelepis, V., 2015. A computational study on the performance and emission parameters mapping of a ship propulsion system. Proceedings of the Institution of Mechanical Engineers, Part M: Journal of Engineering for the Maritime Environment, 229(1), pp.58–76.

Tsakonas, S., 1958. Analytical Expressions for Thrust Deduction and Wake Fraction for Potential Flows. Ship Research, pp.50–59.

Viviani, M. et al., 2008. Marine propulsion system dynamics during ship manoeuvres. 6th International Conference on

high-performance marine vehicles (Hiper 2008), (18–19 September 2008), pp.81–93.
White, F.M., 2009. Fluid mechanics, 7th ed.
Willems, F.P.T., 2000. Modelling and Bounded Feedback Stabilization of Centrifugal Compressor Surge. PhD Thesis, Technische Universiteit Eindhoven.
Yahya, S.M., 2010. Turbines Compressors and Fans, 4th ed., McGraw-Hill.
Yoerger, D.R., Cooke, J.G. & Slotine, J.J.E., 1990. The Influence of Thruster Dynamics on Underwater Vehicle Behaviour and Their Incorporation into Control System Design. IEEE Journal of Oceanic Engineering, 15(3), pp.167–178.
Zhao, F. et al., 2015. An Overall Ship Propulsion Model for Fuel Efficiency Study. Energy Procedia, 75(65), pp.813–818.